International Journal of
MATERIALS RESEARCH

Zeitschrift für METALLKUNDE

Original Contributions

Maryam Abdollahi asl[a], Hamed Ghomi[b]

[a] Department of Tissue Engineering, Najafabad Branch, Islamic Azad University, Najafabad, Iran
[b] Advanced Materials Research Center, Department of Materials Engineering, Najafabad Branch, Islamic Azad University, Najafabad, Iran

Fabrication of highly porous merwinite scaffold using the space holder method

In this study, for the first time, the space holder method was used to fabricate a 3D macroporous nanostructured merwinite scaffold with highly interconnected spherical pores. The nanostructured merwinite powders were prepared by the sol-gel method and an optimal calcination cycle was ascertained. The average values of true and apparent porosities of the prepared scaffolds calculated in the range 85–81 % and 80–74 %, respectively, while the macropore sizes are determined in the range of 400–600 μm. The compressive strength of the prepared scaffold was obtained to be about 0.18–0.29 MPa. Immersion testing in simulated body fluid proved the appropriate bioactivity and biodegradability of the prepared scaffolds. Our study indicated the merwinite scaffold possessed suitable mechanical strength along with highly porous structure and apatite-formation ability which could be used for bone tissue engineering applications.

Keywords: Merwinite; Scaffold; Porous bioceramic; Sol-gel processes; Space holder method

1. Introduction

Bone tissue engineering is one of the advances in medicine that offers solutions for improving and resolving defects and diseases. Scaffolds for bone tissue engineering constitute suitable physical spaces to accommodate cells, and with the exchange of biomolecules encourage the formation of new tissue [1].

Silicate ceramics have characteristics such as biocompatibility, non-toxicity, and stability in the physiological environment of the body. They have made an impressive transformation in the medical world making them promising candidates for bone tissue regeneration [2, 3]. In recent years, merwinite has become known as one of the bioactive silicate ceramics and because of its suitable biological properties (due to magnesium, calcium, and silicon ions in its chemical composition), apatite formation ability, favorable mechanical properties, and convenient degradability rate has attracted much attention [4, 5].

Nanostructured bioceramics, compared with microstructured bioceramics, can lead to stimulation of the reaction between the materials and cells. Also, the crystalline size of nanostructured bioceramics is less than 100 nm. This can improve the adhesion and proliferation of osteoblast cells [6]. In addition, due to the nanosized structure of the natural bones, the use of nanostructured materials can enhance the similarity to the bone and increase the connectivity with bone tissue [7]. With regards to the improved properties, so far limited studies have been done on synthesis and characterization of merwinite bioceramics both in bulk form and as scaffolds [6–8].

Many techniques, such as gelcasting, laser sintering, rapid prototyping, space holder, and polymeric sponge methods, are widely used for manufacturing porous scaffold structures [9]. Among the fabrication techniques, the space holder method has considerable advantages such as low cost, ability to produce scaffolds in final form, independent control of porosity, pore size, and pore morphology, and provides the minimum pore size that can be filled by the

surrounding bone and tissues [10]. This method involves mixing ceramic powder and spacer, compressing the mixture and removing the spacer before, during, or after the sintering process (depending on the type of spacer used).

In this process, the homogeneous mixing of ceramic powder and spacer plays an essential and decisive role in the final properties of the produced scaffold [9, 10]. However, no study has been accomplished on the fabrication of merwinite scaffold by the space holder method.

The present study focuses on the synthesis of nanostructured merwinite by the sol-gel method, and the effect of sintering time and temperature on the purity of merwinite was assessed. Subsequently, porous merwinite scaffolds fabricated via the space holder method and mechanical properties, as well as apatite formation ability and biodegradability of the scaffolds in simulated body fluid (SBF) solution was studied by means of compression tests, scanning electron microscopy (SEM), Fourier-transform infrared spectroscopy (FTIR), and inductively coupled plasma spectroscopy (ICP) techniques.

2. Experimental procedure

2.1. Preparation of merwinite powder

Merwinite powders were synthesized using the sol-gel method. For this purpose, tetraethyl orthosilicate ($(C_2H_5O)_4Si$, TEOS), calcium nitrate tetrahydrate ($Ca(NO_3)_2 \cdot 4H_2O$), and magnesium nitrate hexahydrate ($Mg(NO_3)_2 \cdot 6H_2O$) were used as the starting materials. All these were acquired from Merck Company. Briefly, TEOS with deionized water and two normal HNO_3 [$TEOS/H_2O/HNO_3 = 1:8:0.16$ molar ratio] were mixed with moderate speed and hydrolyzed for 30 min under magnetic stirring.

Subsequently, 0.5 mol magnesium nitrate hexahydrate and 1.5 mol calcium nitrate tetrahydrate were added to the sol solution which was then slowly stirred for 5 h at room temperature. The obtained translucent gel was dried in an air oven at 60 °C for one day and 120 °C for two days.

The powder produced by the sol-gel process was calcined in two cycles. In the first cycle, the powder was heated for 2 h at 700 °C and 3 h at 1 250 °C, and in the second cycle, the powder was heated for 3 h at 1 200 °C. Both cycles were performed in an electrical box furnace using a heating rate of 5 K min^{-1}.

In order to achieve the nanostructured merwinite powder, the calcined powders were milled within a zirconia cup and balls for 10 h at the rotational speed of 250 rpm with a ball to powder ratio of 4/1.

2.2. Preparation of merwinite scaffolds

Sodium chloride particles were used as the spacers. They were separated by sieving and the particles with a size of 420–600 microns were selected.

The weight percentage of the spacer was calculated by using Eq. (1):

$$w_{\text{spacer}} = \frac{V_{\text{spacer}} \times \rho_{\text{spacer}}}{\left(V_{\text{spacer}} \times \rho_{\text{spacer}} + V_{\text{powder}} \times \rho_{\text{powder}}\right)} \times 100 \quad (1)$$

In this equation W_{spacer} is the weight percentage of the spacer, V_{spacer} and V_{powder} respectively are the volume fractions of the spacer and the merwinite powder in the scaffolds. The densities of the sodium chloride (ρ_{spacer}) and merwinite (ρ_{spacer}) are 2.17 and 3.3 g cm^{-3}.

After finding the right ratio, the merwinite powders were mixed with sodium chloride particles and were well homogenized in the amalgamator. The resulting mixture was mixed with 2 wt.% food-grade sunflower oil so that less press pressure is required in deformation and a more homogeneous mixture is obtained.

After that, a suitable amount of the mixture was cold compacted in a cylindrical mold, 10 mm in diameter, using a Universal Testing Machine (SANTAM-STM 150) afterwards they were uniaxially pressed with pressures of 50, 100 MPa. The speed of applying pressure was set to 5 mm · min^{-1}. The final pressure was kept on the mixture for 5 min.

In the next step, the green body of the cold compacted cylindrical samples was sintered at 1 250 °C for 150 min. The heating rate was set at 4 K min^{-1} to prevent thermal shock and cracking of scaffolds. In order to remove the remaining NaCl, after sintering the scaffold was soaked in deionized water for 24 h at room temperature and deionized water was replaced every 6 h. Finally, the scaffolds were dried at ambient temperature.

2.3. Evaluation and characterization of powders and scaffolds

2.3.1. X-ray diffraction analysis

To analyze the phase composition of the synthesized merwinite powders and achieve optimal calcination cycle X-ray diffraction (XRD, Philips Xpert) was used. The X-ray diffractometer was operated with voltage and current settings of 40 kV and 40 mA, respectively and used Cu-K_a radiation (λ Cu-K_α = 0.154186 nm) in the 2θ range from 20 to 80°.

The grain size of the milled merwinite powders was measured by evaluating the XRD peaks using Eq. (2) (Williamson–Hall equation [11]):

$$\beta \cos\theta = 0.89\lambda/d + 2\varepsilon \sin\theta \quad (2)$$

β is the full width of the diffraction peak under consideration (rad) at half maximum intensity, λ (nm) is the wavelength of the X-ray and θ (°) is the Bragg diffraction angle. Accordingly, when plotting $\beta \cos\theta$ against $\sin\theta$, a straight line with the intercept ($0.89\,\lambda/d$) and slope of $2\,\varepsilon$ was obtained in which ε shows the amount of residual strain. Then the average grain size (d) could be calculated in (nm).

2.3.2. Scanning electron microscopy analysis

The size, morphology, and interconnectivity of the pores of the scaffolds were studied by SEM, Philips XL 30, at an accelerating voltage of 15 kV. For SEM analysis, scaffolds were coated with a thin layer of gold (Au) by sputtering to enhance the contrast. The images were analyzed for the pore size distribution by measuring the diameters of a minimum of 100 pores.

2.3.3. Porosity measurement

The Archimedes method was used to measure the porosity of merwinite scaffolds [12]. For this measurement water as the liquid medium and scaffolds with a height of 12 mm and a diameter of 6 mm were used. The apparent or interconnected porosity was obtained through the following formulation:

$$\text{Interconnected porosity} = [(W_w - W_d)/(W_w - W_s)] \times 100 \quad (3)$$

Where W_w is the weight of the scaffold with water, W_d is the weight of the scaffold and W_s is the weight of the sample hanging in the water.

Total porosity or true porosity which includes the interconnected and the closed porosities was calculated by the Eq. (4):

$$\text{Total porosity} = [1 - [W_d/(\rho(W_w - W_s))]] \times 100 \quad (4)$$

Where ρ is the true density or specific gravity of the ceramic which is equal to 3/3 g cm^{-3}. The results were reported based on an average of three scaffolds.

2.3.4. Mechanical testing

The mechanical properties of the merwinite scaffolds were evaluated by conducting compressive strength tests. The compression test is well suited to characterizing the mechanical properties of porous ceramics and has been generally recognized [13]. The mechanical behavior of the sintered cylindrical-shaped samples (10 mm in diameter and 15 mm in height) was measured by universal testing machine (Hounsfield: H50 KS), loaded at a crosshead velocity of 0.5 mm min^{-1}. The load was applied until the first crack appeared on the scaffolds. Five samples of each type were characterized, and the average was reported.

2.3.5. Bioactivity and biodegradability evaluation

Merwinite scaffolds were immersed in SBF at 36.5 ± 1 °C for 28 days to evaluate the bioactivity and biodegradability. The SBF was prepared and used according to the procedure described by Kokubo et al. [14]. Scaffolds for the immersion test (13 mm diameter, 4 mm height) were produced by the same process as described above.

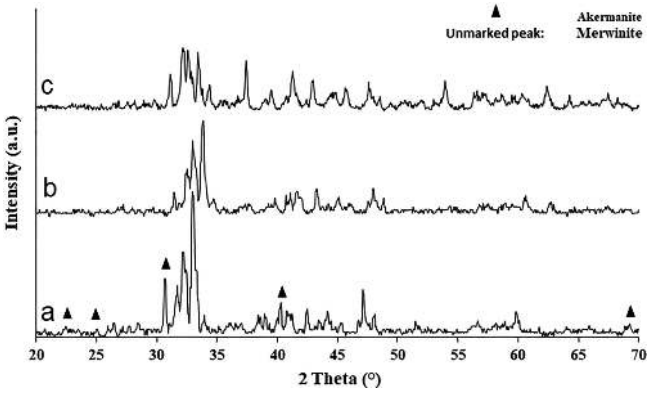

Fig. 1. XRD patterns of the prepared merwinite nanopowder sintered (a) at 700 °C for 2 h afterward at 1 250 °C for 3 h, (b) at 1 200 °C for 3 h, and (c) at 1 200 °C for 3 h and milling for 10 h.

The prepared specimen was immersed in 15 ml of the SBF, and the SBF solution without scaffold was considered as a control. After soaking for the prescribed periods, the soaked samples were removed from the solution rinsed gently with deionized water and dried at room temperature.

Extracts obtained by filtration of the solution were analyzed using ICP, ARL instruments for the determination of calcium, magnesium, silicon and phosphorous ions concentrations. Also, the level of these ions was measured in the control sample solution.

The formation and morphology of precipitates on the surface of the scaffolds were investigated by SEM. The precipitates formed on the scaffolds were characterized by FTIR spectroscopy in the range 400–4 000 cm^{-1} region with 2 cm^{-1} resolution. Samples for this analysis were scraped from the surface of the scaffolds to ensure any formation of the surface layer was detected.

Then to avoid spectral reflectance, this material was diluted and ground in KBr with a sample to KBr dilution ratio of 1 : 100.

3. Results and discussion

The calcination temperatures and the phase composition of raw materials were significant factors affecting the crystalline phase and properties of the merwinite ceramic [15]. In the present study, two sintering cycles were used.

Figure 1 shows the XRD patterns of the initial merwinite powder. Figure 1a shows the XRD pattern of the prepared merwinite powder after sintering with the first cycle. As can be seen from the figure, an intense merwinite peak at about 33.60 indicated the main phase of the merwinite. However, the calcined powder contained akermanite ($Ca_2MgSi_2O_7$) phase as an impurity. Figure 1b shows the XRD pattern of the prepared merwinite powder after sintering with the second cycle, which indicated no impurity or secondary phase by decreasing the sintering temperature to 1 200 °C. Only merwinite peaks were present in the patterns of the synthesized powder after sintering with the second cycle (JCPDS 01-074-0382) proving a pure merwinite phase.

Figure 1c shows the XRD pattern of merwinite powder sintered at 1 200 °C for 3 h after milling for 10 h. Increasing the background and decreasing the intensity of some peaks compared to the X-ray diffraction pattern before the milling process indicates the merwinite has become more amorphous or distorted. Also, the crystallite sizes of the sintered powders after 10 h milling process were estimated at 31 nm.

It should be noted that the cytophilicity improved in nanostructured bioceramics in comparison with micro-grained ones. Nanobioceramics facilitate the regeneration of periodontal ligament cells through the remodeling of alveolar bone. Many studies have confirmed the significance of manufacturing bio-ceramics in nanoscale structures for bone tissue engineering [7, 10].

Scanning electron micrographs of the prepared scaffolds of merwinite are shown in Fig. 2. These figures showed the fabricated scaffolds had well-ordered spherical pores, and interconnection between the pores with a dendritic structure that formed uniformly throughout the scaffolds.

Scaffolds with heterogeneous pores induce cell adhesion in a non-uniform manner. The tissues produced from the

scaffolds with inhomogeneous porosity, as compared to the tissues derived from that with uniform pore structure, have poor biochemical properties [16].

Sodium chloride particles were selected as the spacer due to their high hardness. They keep their original shape and morphology and do not undergo distortion during the sintering and compaction processes. Also, they have low cost, dissolve rapidly in water and create the spherical morphology proportional to the size range of the selective spacer particles [17]. Moreover, since the ideal scaffold for tissue engineering applications should have at least 80 % porosity, the sodium chloride volume percentage was adjusted at 80 % [18].

The results of the image analysis of SEM micrographs showed that the scaffolds had a uniform pore size distribution between 400 – 600 µm with an average pore diameter of 450 µm. The pore size is essential for bone tissue engineering applications so that interconnected pores with a size of more than 300 µm are recommended for improving cell seeding, the formation of capillaries, more excellent tissue ingrowth and formation of new tissue [17, 18].

Also spreading and proliferation by bone progenitors were able to fill 400 µm pores within two weeks [19].

SEM micrographs in higher magnification are shown in Fig. 2c and d. The red circles in Fig. 2c indicate the micropores (<50 µm) on the wall of the macropores which enhance bioactivity and biodegradability by increasing the release of ionic products. These features increase new bone formation and are required for immediate protein and cell migration, cell adhesion, osteointegration, nutrient delivery and waste removal [19, 20].

Table 1 shows the effect of compaction pressure on compressive strength and the average values of true (total) and apparent (interconnected) porosities in the scaffolds.

The average values of true and apparent porosities of the prepared scaffolds were calculated in the range of 80 – 85 and 74 – 81 %, respectively.

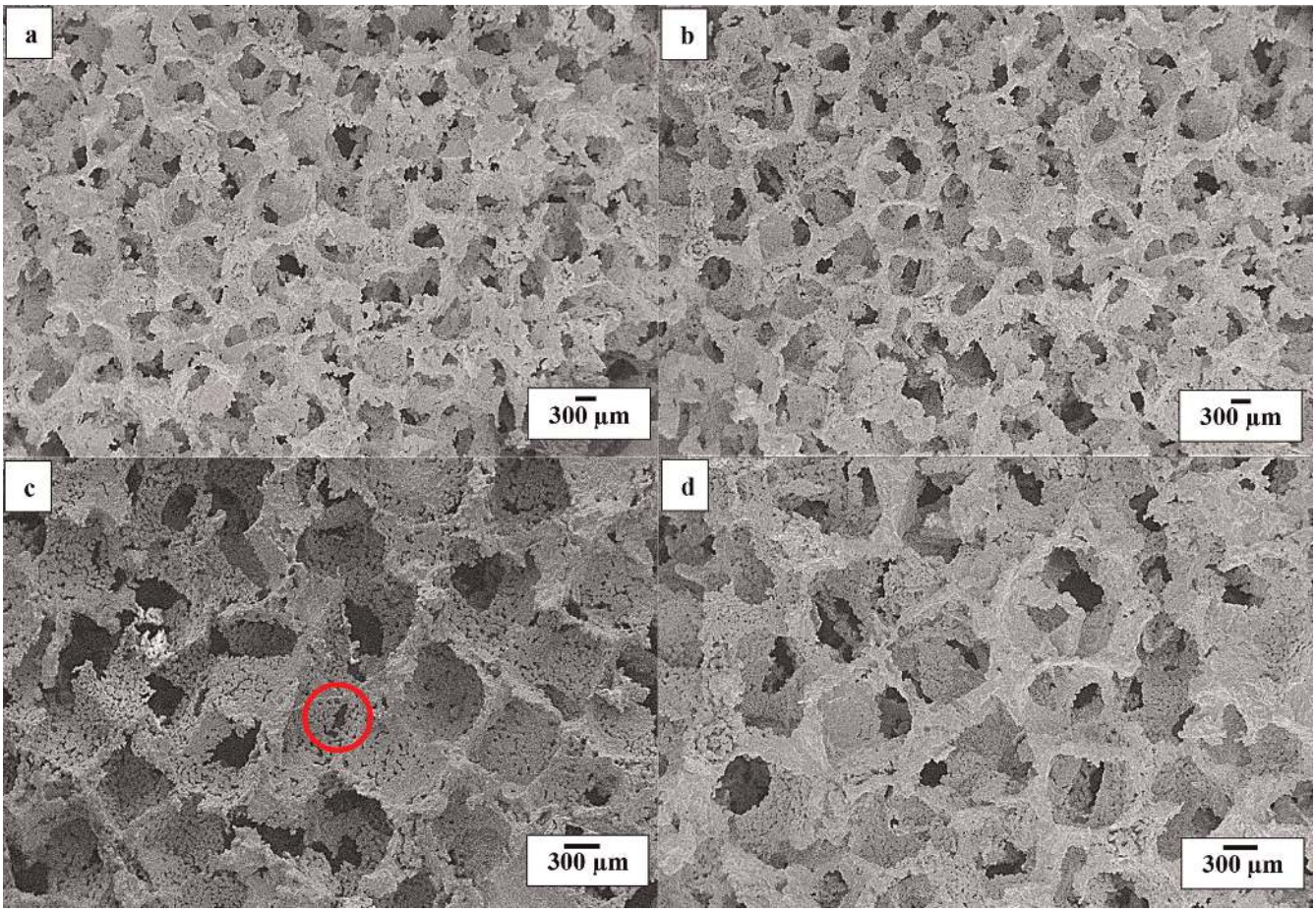

Fig. 2. SEM micrographs at different magnifications of the prepared merwinite scaffolds sintered at 1 200 °C for 3 h shows the well-ordered spherical pores.

Table 1. True and apparent porosity and compressive strength of the merwinite scaffolds processed at different press pressures.

Pressure (MPa)	Compressive strength (MPa) (S.D.)[1]	True porosity (%) (S.D.)	Apparent porosity (%) (S.D.)
50	0.18 (± 0.04)	85 (± 0.48)	85 (± 0.48)
100	0.29 (± 0.05)	81 (± 0.67)	74 (± 0.56)

[1] Standard deviation

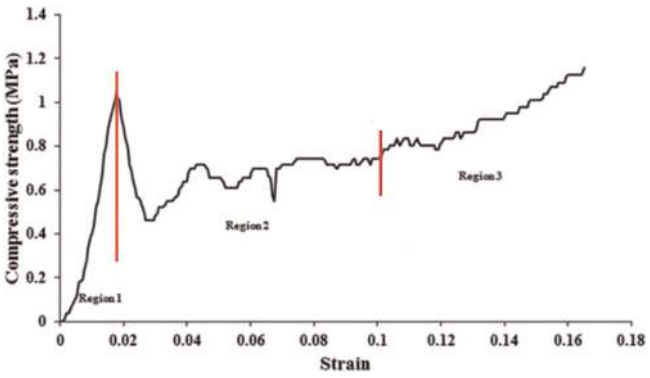

Fig. 3. A compressive stress/strain curve of the typical behavior of merwinite scaffolds.

The results showed that by enhancing the compaction pressure from 50 to 100 MPa, alongside decrement in total porosity, the interconnected porosity was decreased from 81 to 74 %. In fact, by increasing the compaction pressure in addition to decreasing the porosity and macropore size, also the size and number of the micropores which existed on the pore wall and pore boundary were reduced.

Highly porous bioceramic scaffolds have been used as templates for bone growth in three-dimensional space [21]. In addition, they possess a large surface area, which favors cell attachment and tissue growth. Porosity in different materials, ranging from 40 % to 90 %, promotes osteointegration with the implant surface and enhances a mechanical interlock of the implant [22].

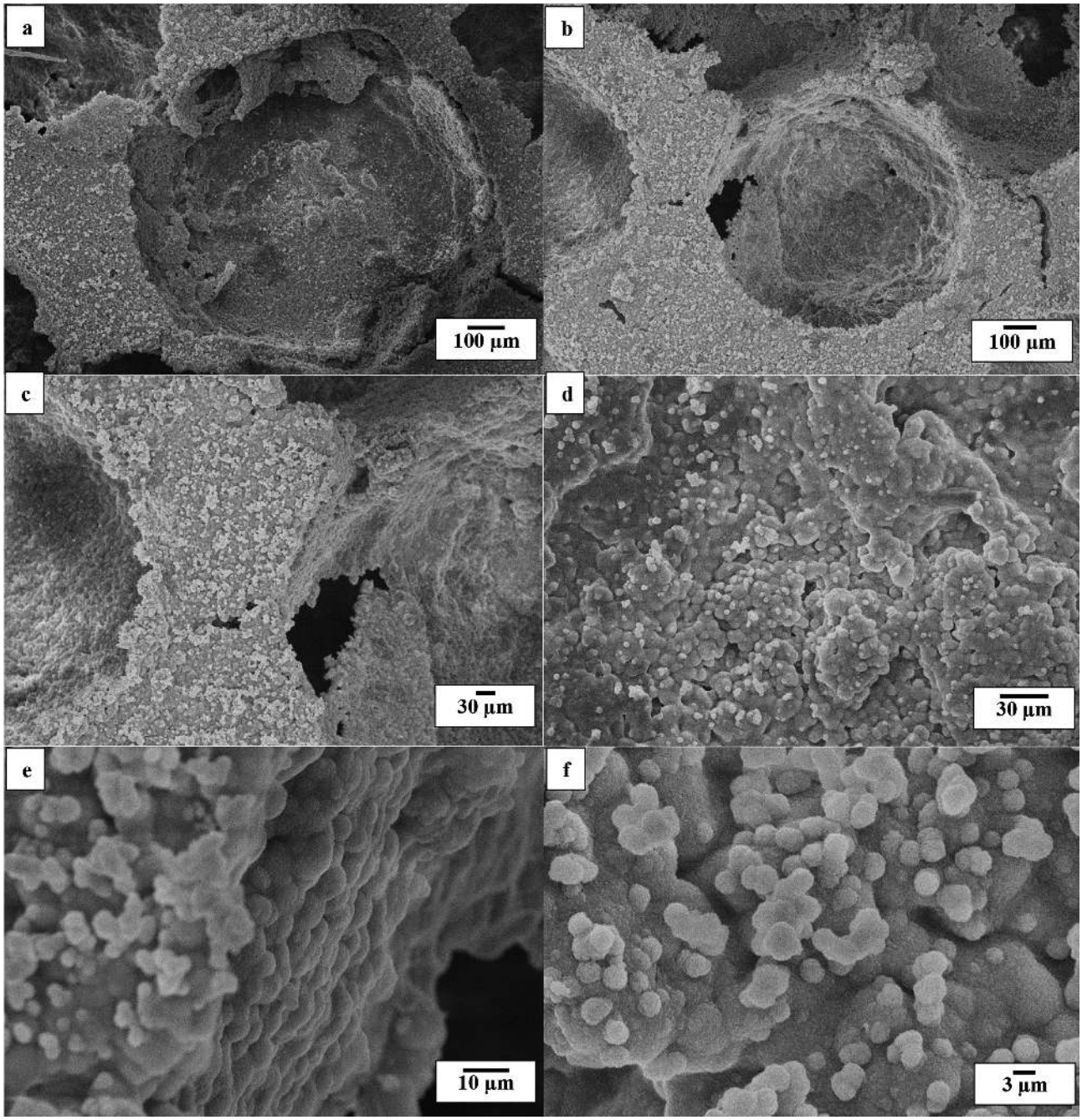

Fig. 4. SEM micrographs at different magnifications of the prepared scaffold after immersion in SBF solution for 28 days shows the formation of the bone-like apatite on the surface and inner wall of the pores.

Since increasing the porosity and pore size results in a decrease in strength, maintaining a balance between the optimal porosity percentage and mechanical strength is essential. In this study, by increasing the compacting pressure on average, the compressive strength of scaffolds was increased by 1.6 times. This result is evidently due to the decrease in the porosity and pore size.

Additionally, according to studies, bone ingrowth enhances the compressive strength of the porous scaffolds in the in-vivo environment [23]. Thus the scaffolds must have only a minimum adequate strength to be appropriately modified for the application of tissue engineering, and it is not essential to manufacture a scaffold with mechanical strength equal to the natural bone [24, 25].

Figure 3 shows a compressive stress/strain curve of the typical behavior of merwinite scaffolds consisting of three separate regions. Region I of the graph is the linear elastic part, which in samples pressed under the 100 MPa pressure is longer and has a higher elastic modulus. This region continued until the maximum compressive strength and ended when the scaffolds fail. Region II defined persistent failure of the walls of the pores until almost struts have fractured and pores collapse. In region III, compaction of the fractured scaffold indicated by further enhancing the stress.

The strength of the fabricated scaffolds were adequate to withstand the forces during handling and immersion in the SBF. In order to evaluate the bioactivity and biodegradability, the scaffolds with 85 % porosity were immersed in SBF. Figure 4 shows SEM micrographs of the scaffolds after soaking in the SBF solution for 28 days.

Bone-like apatite covered the surface and inner wall of the pores. High magnifications show that the bone-like apatite has tiny spherical particles with sizes in the range 200–500 nm in diameter. In addition, small particles can also be seen which represented crystallization nuclei and confirmed the formation of apatite layer during a few days of immersion in SBF [26].

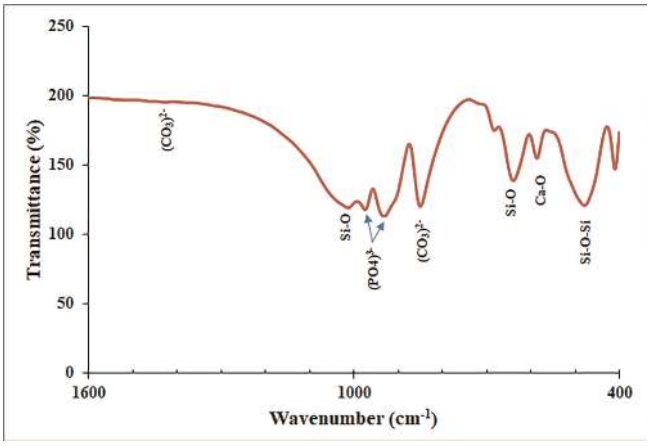

Fig. 5. FTIR spectrum of the precipitates formed on the merwinite scaffolds after soaking in SBF solution for 28 days.

Figure 5 illustrates the FTIR spectrum of the merwinite scaffold after immersion in SBF for 28 days.

The band at about 475 cm^{-1} corresponds to the vibrational mode of the bending of Si–O–Si. The Ca–O band at 586 cm^{-1} and the Si–O bands at 639 and 680 cm^{-1} also observed [27, 28]. In addition, the symmetric stretching at 1 010 cm^{-1} is assigned to the vibrational mode of bending Si–O–Si [29].

The band at 1 636 cm^{-1} arises from intercalated H_2O and the band at 3 428 cm^{-1} is due to the stretching mode of hydrogen-bonded OH^- ions. Two vibrational modes are visible for the $(PO_4)^{3-}$ ions in apatite layer, ν_1 $(PO_4)^{3-}$ at 970 and ν_3 $(PO_4)^{3-}$ at 933 cm^{-1} [7, 30, 31]. Absorption peaks at about 853 cm^{-1} and 1 420 cm^{-1} assigned to the ν_2 and ν_3 band of carbonate were also observed. Presence of carbonate peaks indicated that $(PO_4)_3^-$ sites on the apatite structure were partially substituted by carbonate ions [32]. The above result confirmed that the formed apatite layer was carbonate hydroxyapatite (HA).

Carbonate HA formation on the surface of bioactive materials, due to its similarity to biological apatite, ensures the bone regeneration in in-vivo conditions [33].

The significant criterion for bioactive materials, providing the ability to bond with the living bone, is the formation of a surface bone-like apatite layer in a biomimetic environment [34]. The created bone-like apatite layer can provide a favourable environment for osteoblasts or osteoprogenitor cells and promoting the regeneration of the bone tissue [35]. In the present study, thick layer formation of apatite on the surface and inner wall of the pores confirmed the high degree of bioactivity of the scaffold.

Table 2 shows values of the Ca, Mg, and Si and P concentrations in SBF solution after soaking the scaffolds for 28 days.

In comparison with the values obtained from the control, the concentration of calcium, magnesium, and silicon ions was increased in the SBF solution after immersion of merwinite scaffolds, which confirms the high degradability of the prepared scaffolds. In contrast, the concentration of phosphorus decreased as a result of the apatite formation during this time.

A significant increase in calcium ion concentration indicates that although the formation of the apatite layer is accompanied by the use of calcium ions, the release of calcium ions from the destruction of merwinite has a higher rate than calcium ion consumption. This result is due to the fact that merwinite is a type of orthosilicate and can be hydrolyzed faster than other silicate species (e. g. disilicates, chain silicates) [36, 37].

Studies have shown that the release of magnesium and silicon ions from silicate ceramics stimulates osteoblast proliferation and differentiate genes and plays a critical role in bone remodeling [38]. Also, magnesium is one of the essential elements in the body that contributes to the mineralization process of bone tissue and induces angiogenesis during bone regeneration [39].

Table 2. Values of the Ca, Mg, Si and P concentrations in SBF solution before and after soaking the scaffolds for 28 days.

element	Ca	Mg	Si	P
Concentration in SBF before immersion (ppm)	153.8	58.39	81.83	5
Concentration in SBF after immersion for 28 days (ppm)	677.7	142.7	768.67	3.93

In recent years highly porous scaffolds have received great attention. Porous scaffolds act as a template for tissue growth and have been used in extensive applications such as bone defect filling and implant fixation via bone ingrowth. Meanwhile merwinite is well-known as one of the silicate ceramics because of many distinct advantages, such as good bioactivity, favourable biodegradability, and releasing silicon and magnesium ions which encourage the growth, differentiation, adhesion, and proliferation of the osteoblast cells [40].

In this study, the highly porous nanostructured merwinite scaffold fabricated had a uniform and spherical interconnected pore network with adequate pore size, good mechanical strength, along with sufficient bioactivity and biodegradability thereby being a promising candidate for use in bone tissue engineering.

4. Conclusions

In the present work, for the first time, the space holder technique was used to fabricate nanostructured highly porous three-dimensional merwinite scaffolds. The prepared scaffolds have well-ordered spherical pores and displayed a monotonic distribution of interconnected macropores with a pore size mainly about 400–600 μm. According to the results, by increasing the compaction pressure from 50 to 100 MPa, compressive strength was enhanced from 0.18 to 0.29 MPa while the average values of total and interconnected porosities were obtained in the range of 80–85 and 74–81 %, respectively. The nano-sized structure and the high amount of macropores with several micropores observed in the scaffolds can create the conditions to enhance bioreactions and hence, increase the bioactivity and biodegradability. According to the ICP analysis, the decrease in phosphorus content as a result of the precipitation of an apatite layer on the surface and inner wall of the pores after 28 days of immersion process showed the high degree of bioactivity. Also, increasing the content of magnesium, silicon and calcium in the SBF solution confirms the high biodegradability of the prepared scaffolds. These properties could make the merwinite scaffold a promising candidate for bone tissue engineering and restoration of bone defects.

The authors thank the Islamic Azad University (Najafabad Branch) for providing the facilities for this research.

References

[1] H. Ghomi, R Emadi. Sh. Haghjooye Javanmard: Mater. Des. 91 (2016) 193–200. DOI:10.1016/j.matdes.2015.11.078
[2] A.l. Caplan: Tissue Eng. Part A 25 (2019) 515–517. PMid:30654728; DOI:10.1089/ten.tea.2019.0011
[3] A. Nadernezhad, F. Moztarzadeh, M. Hafezi, H. Barzegar-Bafrooei: J. Eur. Ceram. Soc. 34 (2014) 4001–4009. DOI:10.1016/j.jeurceramsoc.2014.05.014
[4] M. Hafezi, A. Talebi, M. Miresmaeili, F. Sadeghian, F. Fesahat: Ceram. Int. 39 (2013) 4575–4580. DOI:10.1016/j.ceramint.2012.11.054
[5] H. Ghomi, R. Emadi: Int. J. Mater. Res. 109 (2018) 257–264. DOI:10.3139/146.111597
[6] S. Soleymani Eil Bakhtiari, S. Karbasi, S.A. Hassanzadeh Tabrizi, R. Ebrahimi-Kahrizsangi: Polym. Compos. 40 (2019) 1622–1632. DOI:10.1002/pc.25104
[7] M. Hafezi, F. Moztarzadeh, M. Rabiee, A.R. Talebi: Ceram. Int. 37 (2011) 175–180. DOI:10.1016/j.ceramint.2010.08.034
[8] J. Ou, G.F. Yin, D.L. Zhou, X.C. Chen, Y.D. Yao, W.Z. Yang, B.L. Wu, M. Xue, J. Cui, W.F. Zhu, Y.Q. Kang: Key Eng. Mater. 330 (2007) 67–70. DOI:10.4028/www.scientific.net/KEM.330-332.67
[9] A. Mansouri, N. Muhamad, A. Baker: J. Mater. Process. Technol. 212 (2012) 83–89. DOI:10.1016/j.jmatprotec.2011.08.008
[10] H. Ghomi, R. Emadi, Sh. Haghjooye Javanmard: Mater. Lett. 167 (2016) 157–160. DOI:10.1016/j.matlet.2015.12.161
[11] G.H. Williamson, W.H. Hall: Acta Metall. 1 (1953) 22–31. DOI:10.1016/0001-6160(53)90006-6
[12] D.R. Askeland: The Science and Engineering of Materials, 2nd ed. PWS Pub. Co. (1989).
[13] I. Sabree, J.E. Gough, B. Derby: Ceram. Int. 41 (2015) 8425–8432. DOI:10.1016/j.ceramint.2015.03.044
[14] C. Gerhardt, A.R. Boccaccini: Mater. 3 (2010) 3867–3910. PMid:28883315; DOI:10.3390/ma3073867
[15] W. Sun, C. Chu, J. Wang, H. Zhao: J. Mater. Sci. – Mater. Med. 18 (2007) 677–683. DOI:10.1007/s10854-006-9079-2
[16] S.F. Aida, M. Hijrah, A. Amirah, H. Zuhailawati, A.S. Anasyida: Procedia Chem. 19 (2016) 234–240. DOI:10.1016/j.proche.2016.03.099
[17] B. Arifvianto, J. Zhou: Mater. 7 (2014) 3588–3622. PMid:28788638; DOI:10.3390/ma7053588
[18] S. Sadeghzade, F Shamoradi, R. Emadi, F. Tavangarian: J. Mech. Behav. Biomed. Mater. 68 (2017) 1–7. PMid:28135637; DOI:10.1016/j.jmbbm.2017.01.034
[19] C.M. Murphy, M.G. Haugh, F.J. Obrien: Biomater. 31 (2010) 461–466. PMid:19819008; DOI:10.1016/j.biomaterials.2009.09.063
[20] E.A. Aguilar-Reyes, C.A. Leon-Patino, B. Jacinto-Diaz: J. Am. Ceram. Soc. 95 (2012) 3776–3780. DOI:10.1111/j.1551-2916.2012.05465.x
[21] M. Okamoto, in: Handbook of Tissue Engineering Scaffolds, Vol. 1, Woodhead Publishing (2019) 23–49. DOI:10.1016/B978-0-08-102563-5.00002-2
[22] V. Karageorgiou, D. Kaplan: Biomater. 26 (2005) 5474–5491. PMid:15860204; DOI:10.1016/j.biomaterials.2005.02.002
[23] A. Najafinezhad, M. Abdellahi, H. Ghayour, A. Soheily, A. Chami, A. Khandan: Mater. Sci. Eng., C 72 (2017) 259–267. PMid:28024584; DOI:10.1016/j.msec.2016.11.084
[24] C. Wu, Y. Ramaswamy, H. Zreiqat: Acta Biomater. 6 (2010) 2237–2245. DOI:10.1016/j.actbio.2009.12.022
[25] J. Yanpeng, L. Zonghua, Z. Changren, F. Cui: Front. Mater. Sci. China 1 (2007) 140–146. DOI:10.1007/s11706-007-0025-x
[26] R.K. Iler: "Colloid chemistry of silica and silicates", Cornell University Press, Ithaca, New York, 1955. DOI:10.1002/ange.19560680824
[27] W.Y. Zhai, H.X. Lu, L. Chen, X. Lin, Y. Huang, K. Dai, K. Naoki, G. Chen, J. Chang: Acta Biomater. 8 (2012) 341–349. PMid:21964215; DOI:10.1016/j.actbio.2011.09.008
[28] A.R. Oki, B. Parveen, S. Hossain, S. Adeniji, H. Donahue: J. Biomed. Mater. Res. Part A 69 (2004) 216–221. PMid:15057994; DOI:10.1002/jbm.a.20070
[29] I. Michailova, L. Radev V. Aleksandrova, I.V. Colova, I.M.M. Salvado, M.H.V. Fernandes: Bulgarian Chem. Commun. 47 (2015) 253–260. WOS:000367650000039.
[30] C. Soundrapandian, S. Datta, B. Kundu, D. Basu, B. Sa: Am. Assoc. Pharm. Sci. 11 (2010) 1675–1683. PMid:21107772; DOI:10.1208/s12249-010-9550-5
[31] A. Martinez, I. Izquierdo-Barba, M. Vallet-Regi: Chem. Mater. 12 (2000) 3080–3088. DOI:10.1021/cm001107o
[32] P. Valerio, M.M. Pereira, A.M. Goes, M.F. Leite: Biomater. 25 (2004) 2941–2948. PMid:14967526; DOI:10.1016/j.biomaterials.2003.09.086
[33] Ch. Wu, Y. Ramaswamy, H. Zreiqat: Acta Biomater. 6 (2010) 2237–2245. DOI:10.1016/j.actbio.2009.12.022
[34] T. Tithito, P. Suntornsaratoon, N. Charoenphandhu, J. Thongbunchoo, N. Krishnamra, I.M. Tang, W. Pon-On: Biomed. Mater. 14 (2019) 025013. PMid:30690438; DOI:10.1088/1748-605X/ab025f
[35] H.M. Yin, X. Li, P. Wang, Y. Ren, W. Liu, J.Z. Xu, J.H. Li, G. Zhong J. Biomed. Mater. Res. Part A 107 (2019) 654–662.
[36] Ch. Wu, J. Chang: Biomed. Mater. 8 (2013) 032001. PMid:23567351; DOI:10.1088/1748-6041/8/3/032001
[37] C. Ohtsuki, T. Kokubo, T. Yamamuro: J. Non-Cryst. Solids 143 (1992) 84–92. DOI:10.1016/S0022-3093(05)80556-3

[38] S. Zou, D. Ireland, R.A. Brooks, N. Rushton, S. Best: J. Biomed. Mater. Res. Part B 90 (2009): 123–130. PMid:19194862; DOI:10.1002/jbm.b.31262
[39] V. Bunpetch, X. Zhang, T. Li, J. Lin, E.P. Maswikiti, Y. Wu, D. Cai, J. Li, S. Zhang, Ch. Wu, H. Ouyang: Biomater. 192 (2019) 323–333. PMid:30468999; DOI:10.1016/j.biomaterials.2018.11.025
[40] A. Cheng, Z. Schwartz, A. Kahn, X. Li , Z. Shao, M. Sun, Y. Ao, B. D Boyan , H. Chen: Tissue Eng. Part B 25 (2019) 14–29. PMid:30079807; DOI:10.1089/ten.TEB.2018.0119

(Received November 6, 2019; accepted May 30, 2020; online since August 13, 2020)

Correspondence address

Dr Hamed Ghomi
Assistant professor
Department of Tissue Engineering
Najafabad Branch, Islamic Azad University
Najafabad
Iran
Tel.: +98 (31) 42292307
Fax: +98 (31) 42292747
E-mail: hamed1985.gh@gmail.com, hamed.ghomi@ma.iut.ac.ir, hamed.ghomi@pmt.iaun.ac.ir
Web: http://research.iaun.ac.ir/pd/ghomi/

Bibliography
DOI 10.3139/146.111937
Int. J. Mater. Res. (formerly Z. Metallkd.)
111 (2020) 9; page 711–718

ISSN 1862-5282